Extended x-ray-absorption fine-structure technique. III. Determination of physical parameters*

E. A. Stern and D. E. Sayers
Department of Physics, University of Washington, Seattle, Washington 98195

F. W. Lytle
The Boeing Company, Seattle, Washington 98124

(Received 23 December 1974)

Fourier transforms of extended x-ray-absorption fine structure (EXAFS) give structural information in the vicinity of each kind of atom, separately, in a wide variety of gaseous, liquid, and solid systems. A detailed description of the analysis of EXAFS data is presented including details of the Fourier transform of the data and the extraction of structrual and other physical parameters from these transforms. Included in this description are the measurement of interatomic distances, coordination numbers, disorder effects (thermal and structural), energy-dependent electron scattering amplitudes, inelastic mean free paths, and phase shifts. EXAFS spectra of Ge, Cu, and GeO_2 are analyzed in detail. Multiple-scattering effects between atoms are generally found to be small. There are no multiple-scattering effects in the first shell of the Fourier transform. The phase shifts introduced by both the absorbing and surrounding atoms empirically appear to be characteristic of the particular atoms and independent of the surroundings for a given class of material. This is of great practical importance because it indicates that EXAFS can be calibrated by measuring known structures and then used to determine unknown ones.

I. INTRODUCTION

The extended x-ray-absorption fine structure (EXAFS) is the oscillation in the absorption coefficient on the high-energy side of x-ray-absorption edges which can extend around 1000 eV past the edge. In two previous papers[1,2] (hereafter referred to as I and II), a somewhat general theory of EXAFS for the K edge and the experimental details were presented, respectively. In this paper, we will present a method for determining the physical parameters from the K-edge data and will illustrate this by a detailed analysis of the data for Ge and Cu. Preliminary results on these materials have been presented previously.[3,4] The case of L-edge EXAFS will be discussed elsewhere.[5]

The physical parameters for EXAFS are obtained by an appropriate Fourier analysis of the data, and details of this analysis are discussed in Sec. II. The parameters determined by EXAFS relate to the local environment surrounding the x-ray-absorbing atom and can locate the kinds, numbers, and types of surrounding atoms. In Sec. III, we interpret the Fourier transforms to determine the various physical parameters. A summary and conclusions are presented in Sec. IV.

II. FOURIER ANALYSIS

In I, it was shown that generally the x-ray absorption near the K edge can be separated into two terms: a smoothly varying term and a normalized interference term $\chi(k)$, which varies nonmonotonically with energy of the photon. In II, the analysis of the absorption data to separate these two terms was described. In this section, we consider the Fourier analysis of the normalized interference term which is the EXAFS. Fourier analysis of this EXAFS determines the spatial variation of a scattering matrix. If multiple-scattering effects between atoms are neglected, then $\chi(k)$ in the limit $kr_j \gg 1$ can be expressed as[1]

$$\chi(k) = \frac{m}{4\pi\hbar^2 k} \sum_j t_j(2k) \int \frac{e^{-2r_j/\lambda}}{r_j^2} \times \sin 2[kr_j + \delta_j(k)]\, p(r_j)\, dr_j \,, \tag{1}$$

where k is the wave vector of the ejected photoelectron, the sum is over the atoms at the distances r_j from the absorbing atom, $t_j(2k)$ is the magnitude of the amplitude for backscattering from the jth atom, λ is the mean free path for electron-electron and other inelastic scatterings, and $p(r_j)$ is the probability that the jth atom is at r_j. The probability distribution $p(r_j)$ is caused by lattice vibrations or disorder. The oscillatory term contains a phase shift δ_j, which is the sum of the contribution of the p-wave phase shift in the absorbing atom potential $\delta_1(k)$ and the phase shift $\phi_j(k)$ in the backscattering amplitude of the jth atom,

$$\delta_j(k) = \delta_1(k) + \phi_j(k) \,. \tag{2}$$

If we assume $p(r_j) = [1/(2\pi)^{1/2}\sigma_j] \exp[-(r - R_j)^2/2\sigma_j^2]$, where R_j is the average position between the origin atom and the jth atom, and σ_j is the root mean square deviation from R_j and is assumed small compared to interatomic distances, then

$$\chi(k) = \frac{m}{4\pi\hbar^2 k} \sum_j \frac{N_j}{R_j^2} t_j(2k)\, e^{-2R_j/\lambda}$$

$$\times \sin 2[kR_j + \delta_j(k)]\, e^{-2k^2\sigma_j^2} , \qquad (3)$$

where now the sum is over the different shells of atoms whose average distance from the absorbing atom is R_j and which contain N_j atoms.

The quantities we ideally want to determine from the data are σ_j, λ, $\delta_j(k)$, N_j, R_j, and $t_j(2k)$. If σ_j is the same for all shells and independent of j, then Eq. (3) has the simple form

$$\chi(k, T) = \chi(k, 0)\, e^{-2k^2\sigma^2(T)} , \qquad (4)$$

where $\chi(k, T)$ is $\chi(k)$ at temperature T, and σ is generally a function of temperature. Thus taking the ratio of χ measured at two different temperatures T_1 and T_2, it is possible to determine

$$\sigma^2(T_2) - \sigma^2(T_1) = (1/2k^2) \ln \chi(k, T_1)/\chi(k, T_2) , \qquad (5)$$

by plotting the ln on the right-hand side of Eq. (5) as a function of k^2 and determining the slope of the resulting straight line.

However, if σ_j is a function of j, then the most covenient way to determine these σ_j and the other physical quantities mentioned above is by Fourier transforming the data. The expressions obtained by Fourier transforming with respect to $\sin 2[kr + \delta_j(k)]$ are given in I. However, in practice, $\delta_j(k)$ is usually an unknown and cannot be included in the Fourier-transforming sine function. Thus, the Fourier transform that is actually taken is

$$\phi_n(r) = \frac{1}{\sqrt{2\pi}} \int_{k_{\min}}^{k_{\max}} k^n \chi(k)\, e^{2ikr}\, dk , \qquad (6)$$

where n is usually either 1 or 3, and $k_{\min}$ and $k_{\max}$ are the minimum and maximum k's, respectively, of the useable experimental data, as will be discussed in more detail below.

When $n = 1$, the transform, which can be related to the spatial variation of a scattering matrix,[1] is found to be highly sensitive to $k_{\min}$, especially in the small r region between the origin and the first shell. This is not surprising because the absorption near the edge is not adequately described by Eq. (3). Only for $k \gtrsim 3$ Å^{-1} are the assumptions leading to Eq. (3) valid, as discussed in I. Another difficulty is defining precisely at what energy with respect to the edge the origin of k should be defined. For example, for a metal, one might expect that the origin of k is roughly the Fermi energy below the edge. Any errors in defining this origin or inner potential would most affect the small k part of $\chi(k)$.

We find empirically that using $n = 3$, the transform, which can be related to a pseudocharge density,[1] is reasonably insensitive to the value of $k_{\min}$ and choice of inner potential. Its physical interpretation is as satisfactory as setting $n = 1$, and its value is more uniquely defined. The $n = 3$ transform weights less the low-energy portion of $\chi(k)$, where the undesirable uncertainties occur, while it weights most the high-energy portion of $\chi(k)$, where Eq. (3) is a better approximation although the signal-to-noise ratio is somewhat poorer. For these reasons, we will employ $\phi_3(r)$ as our standard transform in the rest of this paper.

To perform the Fourier analysis, the data must be transformed from energy to wave-number k space. The transform is given by

$$\hbar^2 k^2/2m = E(k) - E_0(k) , \qquad (7)$$

where $E(k)$ is the energy of the photoelectron measured from the x-ray edge, and $E_0(k)$ is the "inner potential" caused by the atomic potentials and represents the potential "zero" above which the kinetic energy must be added to determine the total energy E. In metals, at low energy, E_0 can be approximated by the Fermi energy, but at higher energies (> 30 eV or so), this is no longer true since the exchange and correlation energies go to zero in a complicated way with increasing energy, and the pseudopotential of the ion cores is energy dependent. This problem is identical to finding the inner potential in LEED, where attempts have been made to calculate or derive[6,7] E_0. Fortunately, the k^3 transform makes the result insensitive to a reasonable choice of E_0.

We have tested the insensitivity of the Fourier transforms to variation in E_0. In transforming the data, we have used both a variable E_0 fitted to the theoretically predicted values and a constant E_0 which represents a rough average of these values. The difference in the results obtained between a variable and constant E_0 is small for all quantities except for the constant phase shift β. Since there is enough uncertainty in E_0 that reliable values of β cannot be obtained in any case, a constant value of E_0 is generally used because of its simplicity.

Multiple scattering between atoms is important at distances

$$r > r_0 = \hbar^2 k/2mE_{02}(k) = [E(k)/E_{02}(k)]\, k^{-1} , \qquad (8)$$

where $E_{02}(k)$ is given by

$$E_{02}(k) = \mathrm{Im} E_0(k) = \frac{2\pi\hbar^2}{m} \mathrm{Im} \sum_j n_j f_j(0) . \qquad (9)$$

Here Im denotes the imaginary past, n_j is the number of atoms per unit volume of the jth component, and $f_j(0)$ is the forward-scattering amplitude for a single atom of the jth component in the solid. Formula (9) is accurate in the cases where the real part of $f_j(0)$ is much larger than its imaginary part[8] or when $|E_0|$ is small compared to E.[9] The result of Eq. (8) follows because the lifetime of the plane wave state of wave number k is $\hbar/2E_{02}(k)$, and during this lifetime, it travels a distance r_0 from the origin. At times greater than or equal to this lifetime, the plane wave state is appreciably

TABLE I. Multiple-scattering lengths r_0 for Ge and Cu. Imaginary parts of the forward-scattering amplitude for a single atom is denoted by $f_2(0)$, and its values presented in atomic units.

E	$f_2(0)$	E_{02} (eV)	r_0 (Å)
		Ge	
27	0.115	0.3	5.6
54	0.492	1.1	13.1
122	1.52	3.42	6.3
218	2.32	5.2	5.5
340	2.63	5.9	6.1
666	2.76	6.2	6.3
		Cu	
54	1.57	6.7	2.1
109	1.88	8.1	2.5
218	2.26	9.7	3.0
408	2.41	10.3	3.8
680	2.44	10.4	4.9

modified by scattering, so that multiple-scattering effects between atoms is no longer negligible. Values of r_0 are also tabulated in Table I. These values are obtained using Pendry's potential for atoms.[10] Although Pendry's results may neglect polarization effects from excited states,[11] the error introduced is mainly in the forward scattering. The contributions to r_0 that we are most concerned with are from wide-angle scattering where Pendry's method is more accurate. If the scattering is highly peaked around the forward direction then Eq. (8) underestimates r_0, since E_{02} includes the low-angle scattering which will not contribute to multiple-scattering effects except in the forward direction. However, Pendry's results do not produce large peaking of scattering in the forward direction, and the estimates of V_0 using his results should be reasonable accurate.

The upper limit k_{max} in Eq. (6) is determined primarily by the experimental range of energies

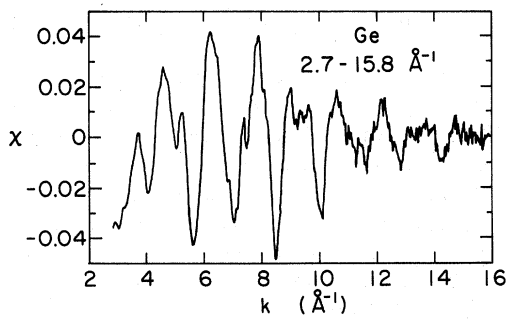

FIG. 1. Normalized EXAFS, $\chi(k)$, vs k (Å^{-1}) for crystalline Ge at 77 °K. Data are shown only in the region 2.7–15.8 Å^{-1}.

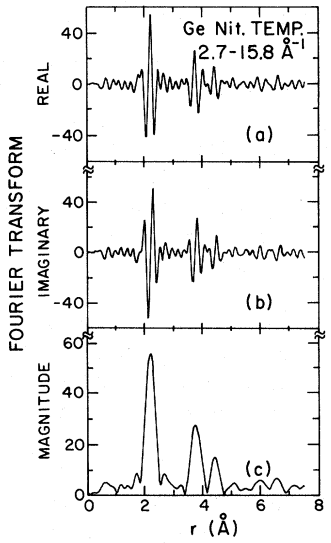

FIG. 2. Real part (a), imaginary part (b), and magnitude (c) of the Fourier transform [i.e., $\phi_3(r)$ from Eq. (6)] of the EXAFS, from Fig. 1, plotted vs r (Å).

above the edge where the EXAFS is discernable above the noise, typically 1000–1500 eV (which corresponds to a k range up to 15–20 Å^{-1}), unless other absorption edges appear in the data. It is usually desirable to have k as large as possible to reduce the termination error found in Fourier transforms which are truncated at finite k.

The Fourier transforms used are the real part (cosine), imaginary part (sine), and magnitude of the transform. In Fig. 1, the EXAFS for crystalline Ge at liquid-nitrogen temperatures over the range to be transformed is shown. Note that the large peak near the edge, as shown in Fig. 8 of II, is not included in calculating the transform. As mentioned in II, this large peak is clearly of a different character from the rest of the EXAFS. Various non-EXAFS explanations of this edge peak are plausible, such as a peak in the unoccupied p-state density of states near E_f, many-body effects, and photoelectron core-hole interaction. However, there is reason to believe that even this edge peak has an EXAFS explanation as backscattering from the conduction electrons between the center atom and first few shells. Since this issue is not resolved as yet, the transformed data do not include the edge peak as indicated in Fig. 1.

In Fig. 2, the transform of the data, $\phi_3(r)$ from Fig. 1, is shown over the range of k from 2.7 to 15.8 Å^{-1} (using $E_0 = -5$ eV), where Fig. 2(a) shows the real part, Fig. 2(b) the imaginary part, and Fig. 2(c) the magnitude of the transform. Corresponding transforms are shown for Cu at liquid-nitrogen temperature and room temperature in Figs. 3 and 4, respectively, over the range of k

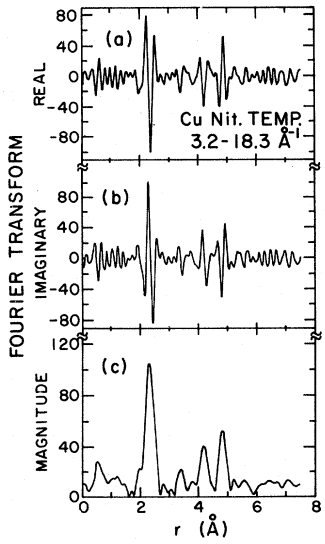

FIG. 3. Real part (a), imaginary part (b) and magnitude (c) of $\phi_3(r)$ vs r (Å) for Cu at 77 °K from the data of Fig. 2 in II. Transform is taken from 3.3 to 18.7 Å^{-1}.

from 3.2 to 18.3 Å^{-1} ($E_0 = -9.5$ eV). The data used to generate $\phi_3(r)$ in Figs. 3 and 4 have been shown in II. The factors which affect the interpretation of these transforms and the information contained in the transforms are discussed in Sec. III.

III. INTERPRETATION

The relationship between the real part, imaginary part, and magnitude of the complex transform of the data ϕ_n of Eq. (6) is apparent in the first large peak in Fig. 2 (between 1 and 3 Å). If the theoretical expression from Eq. (3) is inserted into Eq. (6), and it is assumed that $\delta = 0$, remembering that $t(2k)$ is real, the result would be a symmetric-shaped imaginary part and an antisymmetric real part centered on the shell distance R_j. This is similar to what is observed in Ge for the first shell, except that the real part is symmetric and the imaginary part is antisymmetric, which indicates that the phase δ has a constant part of approximately $\frac{1}{2}\pi$. The structure of the real part consists of a sharp positive peak surrounded by deep negative side lobes; implications of such a shape will be discussed later.

The real and imaginary parts of the transform contain complementary information, so that only one part need be studied. If the width of the peaked structures around each shell is small compared to first-neighbor distances, as is the case for Ge and Cu, then it can be shown that

$$\phi^r(r) = \frac{1}{\pi}\int \frac{\phi^i(r')\,dr'}{r - r'} , \qquad (10)$$

where ϕ^r and ϕ^i are the real and imaginary parts of the radial structure function of Eq. (6).

The situation is somewhat more complicated if δ is equal to an arbitrary finite constant value. By using simple trigonometric identities, it can be shown that the real and imaginary parts now are admixtures of the $\delta = 0$ transforms, so that neither part is completely symmetric or antisymmetric unless the phase is an integral multiple of $\frac{1}{2}\pi$ as for Ge. Location of the peak position may still be made using the magnitude of the transform, since it is independent of any constant phase shift and will be peaked at $r = R_j$. Note that for Ge, the magnitude [Fig. 2(c)] is peaked at the same place as the real [Fig. 2(a)] part, but is smoother and broader since the negative side lobes add to the width in the magnitude.

A. Phase shift

To locate the peak position accurately, it is necessary to understand the phase shift more fully. Estimates of the phase shifts using the WKB method have shown that for many elements the phase shift is approximately linear in k over the EXAFS energy range with a negative slope, i.e.,

$$\delta_j(k) \approx -\alpha_j k + \beta_j , \qquad (11)$$

with α, β constant. This approximate linearity has been verified in the case of Cu using a more exact calculation of phase shifts from a Hartree-Fock potential.[12] Substituting Eq. (11) into Eq. (3) gives the argument for the sine wave of $2k(R_j - \alpha_j) + 2\beta_j$. The effect of constant phase 2β has been discussed above; however, as also pointed out by

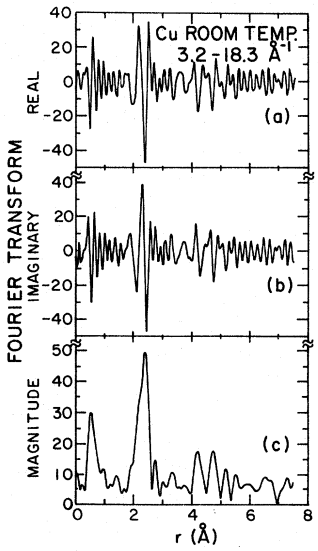

FIG. 4. Same as Fig. 3 for Cu at 300 °K. Amplitudes of Figs. 3 and 4 are referenced to the same scale for direct comparison.

TABLE II. Structural data for Ge and Cu. N_j is the number of atoms in the jth shell, R_j is the true distance and R'_j is the measured distance of the jth shell from the origin, $\alpha_j = R_j - R'_j$ is the coefficient of the term linearly dependent on k in the phase shift. Amplitude of the jth shell is A_j and $B_j/B_1 = N_1 A_j R_j^2 / N_j A_1 R_1^2$.

			Cu nitrogen temp. ($E_0 = -9.5$ eV)				Cu room temp. ($E_0 = -9.5$ eV)			
j	N_j	R_j (Å)	R'_j (Å)	α_j (Å)	A_j	B_j/B_1	R'_j	α_j	A_j	B_j/B_1
1	12	2.56	2.33±0.03	0.23±0.03	104.8±4	1.00	2.42±0.05	0.14±0.05	49.4±4	1.00
2	6	3.62	3.42±0.03	0.20±0.03	22.2±4	0.85±0.19	3.34±0.19	0.28±0.05	11.0±4	0.89±0.40
3	24	4.43	4.20±0.03	0.23±0.03	40.9±4	0.58±0.08	4.20±0.05	0.23±0.05	17.5±4	0.53±0.16
4	12	5.11	4.84±0.03	0.27±0.03	52.7±4	2.01±0.23	4.75±0.05	0.36±0.05	17.6±4	1.42±0.44
5	24	5.72	5.58±0.05	0.14±0.05	13.2±4	0.31±0.11	5.53±0.10	0.19±0.10	10.0±4	0.50±0.24
6	8	6.26	6.17±0.05	0.09±0.05	9.9±4	0.85±0.38	5.93±0.10	0.33±0.10	6.8±4	1.23±1.18
7	48	6.76	6.44±0.05	0.32±0.05	13.2±4	0.22±0.08	6.53±0.10	0.23±0.10	8.8±4	0.31±0.17
			Ge nitrogen temp. ($E_0 = -5$ eV)				Ge nitrogen temp. (Variable E_0)			
j	N_j	R_j	R'_j	α_j	A_j	B_j/B_1	R'_j	α_j	A_j	B_j/B_1
1	4	2.45	2.20±0.03	0.25±0.03	55.6±1.5	1.00	2.18±0.03	0.27±0.03	54.8±1.5	1.00
2	12	4.00	3.77±0.03	0.23±0.03	27.6±1.5	0.44±0.04	3.72±0.03	0.28±0.03	26.7±1.5	0.43±0.64
3	12	4.68	4.43±0.03	0.25±0.03	15.1±1.5	0.33±0.04	4.39±0.03	0.29±0.03	14.9±1.5	0.33±0.04
MS			5.10		4.9±1.5		5.04		4.9±1.5	
4	6	5.65	5.49±0.05	0.16±0.05	2.8±1.5	0.18±0.10	5.45±0.05	0.20±0.05	2.4±1.5	0.16±0.10
5	12	6.16	5.99±0.05	0.17±0.05	5.9±1.5	0.22±0.06	5.97±0.05	0.19±0.05	6.3±1.5	0.24±0.06
6	24	6.92	6.58±0.05	0.34±0.05	6.7±1.5	0.16±0.04	6.53±0.05	0.39±0.05	6.3±1.5	0.15±0.04
7	24	7.34	7.20±0.05	0.14±0.05	3.8±1.5	0.10±0.04	7.11±0.05	0.23±0.05	3.9±1.5	0.11±0.05

Mott,[13] the linear k dependent term shifts the "frequency" of the sine wave from R_j to $R_j - \alpha_j$. In the Fourier transform, this has the effect of shifting all peaks toward the origin by an amount α_j. In crystalline materials where the distances R_j are known, the transforms may be used to evaluate α_j. In Table II, the data for the transforms shown in Figs. 2–4 are tabulated. Table II shows that for the first three shells where the data are most reliable, a value of $\alpha = 0.25 \pm 0.03$ Å may be used for Ge and 0.22 ± 0.03 Cu. These data also show at least six shells in Ge may be located, although there are other features in the data at ~5 and 6 Å which cannot be explained by the model that leads to Eq. (3). These features have recently been shown to be due to multiple scattering between atoms.[14] Both these features occur at distances comparable to r_0 for Ge, as tabulated in Table I where multiple scattering between atoms is expected to be important.

One might question whether the last three peaks indicated by the arrows in Fig. 2 are significant and are not caused by noise or cutoff effects. The reality of the last three peaks can be ascertained by varying the cutoff limits in k space of the EXAFS data before transforming into r space. The invariance of these peaks, compared to the surrounding and smaller structure, shows that these are not spuriously caused by cutoff effects. Their magnitudes are significantly larger than the surrounding noise, and their location coincides with the values predicted by the known structure of Ge. The value of α which can be determined from known structures is typically accurate to ±0.03 Å, which gives a total accuracy of the order of 2% in the absolute distance measurements.

Uncertainty in peak positions may also arise because of errors ΔE of a few eV in E_0. We have carefully evaluated the effects of these errors on the transforms by systematically varying a constant value E_0 and observing the resulting effects in addition to permitting E_0 to be a function of k. We have found that changes of a few eV in a k-independent E_0 cause only slight shifts in the positions of the structural peaks (< 2%) but may have a large effect on the constant phase β_j of each peak as mentioned previously.

When Eq. (11) holds for $\delta(k)$, $\phi_n(r)$ in Eq. (6) can be written

$$\phi_3(r) = \frac{m}{4\pi\hbar^2} \sum \frac{N_j}{R_j^2} e^{-2R_j/\lambda} T_j(r - R_j + \alpha) e^{i\beta} , \qquad (12)$$

where

$$T_j(x) = \int k^2 t_j(2k) e^{-2\sigma_j^2 k^2} e^{i2kx} dk .$$

If $\delta_j(k)$ cannot be accurately described by Eq. (11) but has further dependence on k, the proof that a constant phase can be chosen to make $\phi(r)$ symmetric or antisymmetric about the center of each shell no longer holds, and $\phi(r)$ no longer can be made symmetric or antisymmetric about R_j. We have found that in some systems, there are significant deviations from the linear phase shift dependence in Eq. (11). As shown in Fig. 5, the $\phi_3(r)$ around the position of the first oxygen atom shell in GeO_2 is neither symmetric nor antisymmetric, indicating that the phase shift in the backscattering amplitude cannot be approximated by Eq. (11). It should be emphasized that even though the phase shift in GeO_2 is not linear, the use of crystalline GeO_2 as a standard reference still allows reliable comparison of changes in the first shell in the amorphous polymorph. As an example of this, we

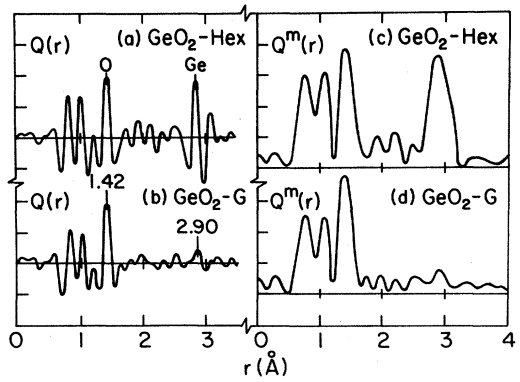

FIG. 5. Real part (a and b) and magnitude (c and d) of $\phi_3(r)$ for crystalline (Hex) and amorphous (G) GeO_2. Shape of the structure at 1.4 Å due to the first-neighbor oxygen atoms arise from a nonlinear phase shift as described in the text. Structure at 2.9 Å is due to the second-neighbor Ge atoms, and its shape is consistent with a linear phase shift as given by Eq. (11).

will determine later on the difference in disorder in the Ge-O distance between the crystalline and glassy states.

It should be pointed out that the second shell in GeO_2, composed of Ge atoms, does have a shape which is similar to crystalline Ge, showing that the $\delta(k)$ for a photoelectron from Ge has the form of Eq. (11) in scattering from another Ge atom, irrespective of the surroundings. The α determined for this second shell is 0.27 Å, as compared to the value of 0.25 Å for pure Ge. The difference between these two values is within the variation of 0.03 Å coming from the uncertainty of E_0.

From these examples of Ge atoms in pure Ge and in GeO_2, we find that the phase shift has the property of being the same independent of the surroundings, at least for covalent structures. Preliminary examination of many other covalent structures containing Ge appears to be consistent with this observation. The phase shift for a photoelectron excited from a Ge atom and scattered from a surrounding Ge atom has the form of Eq. (11) with $\alpha = 0.26 \pm 0.03$, at least for the first few shells where multiple-scattering effects are negligible.

As indicated above, the scattering from oxygen in GeO_2 has a phase-shift k dependence more complicated than the linear dependence of Eq. (11). Remembering from Eq. (2) that the phase shift $\delta_j(k)$ is composed of two contributions, one from the x-ray absorbing atom and the other from the backscattering atom, it is clear that the difference in the $\delta_j(k)$ dependence in oxygen comes from the scattering from the oxygen atom.

The results in pure Ge and GeO_2 suggest the following hypothesis which is consistent with the limited data we have available to date and which should be checked further as more data are accumulated. The hypothesis is also consistent with theoretical considerations to be described shortly. The contribution to the phase shift for a given atom is the same, independent of the surroundings for a given class of binding. The distinction between different classes of binding is only in regard to the amount of charge transferred onto the atoms or the valence state of the atom. If an atom in a given valence state is neutral, whether it be in a metallic or covalent bonding state, we call it in the same class. We have most evidence for covalent bonding and some for metallic bonding. Atoms bonded ionically, particularly for large negative anions such as O^{--}, F^-, etc., appear to have phase shifts different from their covalently bonded states. Atoms which can bond in different valence states also appear to have differing phase shift between these states.

This conjecture is consistent with theoretical considerations. As indicated by Eq. (2), δ_j has two contributions. For a given absorbing atom, the variation in δ_j comes from $\phi_j(k)$, the backscattering phase shift introduced by the jth atom. At the energies important for EXAFS, backscattering comes from the core of the atom and not its valence electrons. Any change in ϕ_j, thus, must occur because of changes in the core. If the valence state of the atom remains the same, no appreciable change in the core will occur by varying the valence electron distribution (as in metallic to covalent binding) as long as the atom remains neutral. However, transferring valence charge to the atom will affect the core because the changed amount of valence electrons causes a change in the shielding of the nuclear charge. In the same way, changing the valence state of the atom will affect the core, because different valence states shield the nuclear charge differently. The phase shift δ_j, introduced by the absorbing atom, is also mainly determined by the core electrons. The same considerations that affect ϕ_j will also affect δ_j. Thus we conclude that our conjecture has theoretical substance to it.

If our conjecture passes the test of an exhaustive experimental study, it has great practical significance. It would be possible to determine α for all possible combinations of atoms in known classes of structures, and then use this calibration to determine the structure in unknown systems.

B. Effects of disorder

The shape of the peak about each shell is not strongly perturbed by the finite range of integration in Eq. (6). Since typically $k_{max} \gg k_{min}$, the width introduced by the finite range over k is $\Delta r \approx \pi/k_{max}$. Here the width is measured at the point where the peak crosses the origin, and it is as-

sumed that the true form of the peak is a δ function. If the peak shape were only determined by the Gaussian disorder and finite cutoff, the ratio of the side lobe depth to peak height would be ~0.15 instead of ~0.6–0.8, as observed in Ge and Cu. The shape of the peak, then, is determined by the k dependence of $k^2 t(2k)\, e^{-2\sigma^2 k^2}$.

The approximate shape of $e^{-2\sigma^2 k^2}\, t(2k)/k$ for Ge and Cu are the envelopes of the EXAFS shown in Figs. 1 and 2 of II, which increases to a peak about $k = 6$–7 Å^{-1} and decreases at higher k. This envelope also includes temperature effects but as Eq. (4) indicates, these decrease monotonically with k and do not give the peaking which is observed. The transforms of a variety of similar envelope functions have been studied by Waser and Schomaker[15] and shown by them to give peaks with large negative side lobes similar to those in Figs. 2–4.

The form of $k^2 t_j(2k)$ and σ_j can be obtained for known structures such as Ge and Cu by isolating the $\phi_3(r)$ for the jth shell [which we will denote by $\phi_{j3}(r)$] and then Fourier transforming it back to k space by integrating $\int [\phi_{j3}(r)/(2\pi)^{1/2}]\, e^{-2ikr}\, dr$, obtaining what we will call $\chi_j(k)$. By repeating this procedure for a second sample which is similar to the first except for a change in σ_j and/or N_j, a plot of k^2 versus the $\ln|\chi_1(k)/\chi_2(k)|$ gives a straight line whose slope is $2[\sigma_{2j}^2(k) - \sigma_{1j}^2(k)]$ and whose intercept at $k = 0$ is $\ln(N_{1j}/N_{2j})$. This follows from reasoning similar to that leading to Eq. (5). By using Eq. (10) under the same conditions that make Eq. (10) valid, it can be proved that $|\chi_j(k)|$, the magnitude of $\chi_j(k)$, is proportional to $k^2 t_j(2k) \times e^{-2k^2\sigma_j^2}$ with the rapid $\sin 2[kR_j + \delta_j(k)]$ variation eliminated.

We first illustrate this procedure for Cu. From Figs. 3 and 4 and Table II, we can see that at least four peaks can be identified in the Cu spectrum as indicated by the arrows. In Fig. 6, $k^2 t_1(2k) \exp[-\sigma_1(T)^2 k^2]$ is shown for the first shell in copper at $T = 77$ °K and $T = 300$ °K. These data

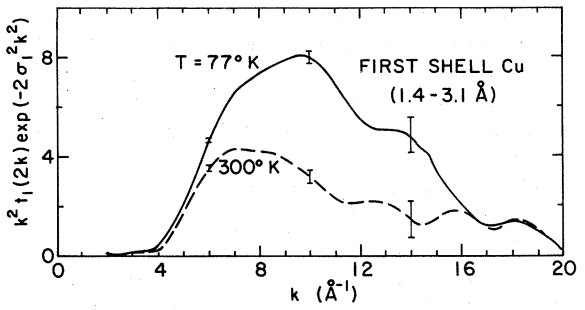

FIG. 6. First shell EXAFS envelopes $k^2 t_1(2k) \exp(-2\sigma_1^2 k^2)$ for Cu vs k (Å^{-1}) at 77 and 300 °K. Reduction of amplitude and shift of the peak from 10 to 7 Å^{-1} in the 300 °K data is due to the increasing disorder.

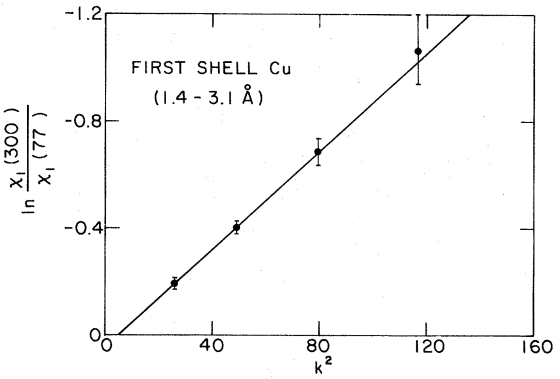

FIG. 7. $\ln[\chi_1(300\,°\text{K})/\chi_1(77\,°\text{K})]$ vs k^2 (Å^{-2}) for the Cu data from Fig. 6. Points plotted represent the maximum number of statistically independent points which may be derived from the data. Below 35 Å^{-2} and above 120 Å^{-2}, there are deviations from the straight line due to finite cutoff in r space (1.4–3.1 Å) and noise, respectively. Equation of the straight line is $-0.0093k^2 + 0.046$.

represent the magnitude of the inverse transform of the data in Figs. 3 and 4 between 1.4 and 3.1 Å. Besides the peaking which is observed at 9.9 and 7.4 Å^{-1} for the $T = 77$ °K and $T = 300$ °K data, respectively, there are peaks which occur above 11 Å^{-1} in both curves. These features at high k are due to noise spikes or small peaks in the data due to inadequate coincidence correction caused by characteristic lines from the x-ray tube which are amplified by the k^3 multiplication of χ. Also shown are typical error bars in different regions in k space. The errors were estimated from the fact that at high k where the curves intersect, the data are dominated by noise. The error bars at lower k are simply scaled down as k^3 from the high-k value.

In Fig. 7, a plot of $\ln[\chi_1(300\,°\text{K})/\chi_1(77\,°\text{K})]$ vs k^2 is shown using the data from Fig. 6 obtaining a straight line between 35 and 120 Å^{-2}. Below 35 Å^{-2}, there is a deviation from a straight line because of truncation effects which affect the data over an interval $\Delta k \sim \pi/\Delta r$ from the lower and upper cutoffs of the data, which were 3.3 and 18.3 Å^{-1}, respectively. Since $\Delta r = 1.7$ Å, this gives $\Delta k \sim 1.8$ Å^{-1}, so that the data should be affected by truncation up to $k = 5$–6 Å^{-1}, as observed. At high k, deviations from linearity occur because of the noise bumps in the data occuring above 11 Å^{-1}. Between 35 and 120 Å^2, only four points are plotted to obtain the straight-line fit. These represent the only statistically independent points which may be plotted in this interval because of the finite resolution Δk described above. The slope of the straight line in Fig. 7 gives for the first shell $\sigma_1^2(300\,°\text{K}) - \sigma_1^2(77\,°\text{K}) = 0.0047 \pm 0.0004$ Å^2 and $N_2 = (1.05 \pm 0.03) N_1$, using the analysis described

above. The value 0.0047 Å^2 is in reasonable agreement with σ_0^2 determined from x-ray measurements of the Debye-Waller factor for Cu. In making this comparison, it must be remembered that in the Debye-Waller factor, the σ_0^2 is for a single atom about its average value, while for EXAFS σ_1^2 is the relative displacement between the origin atom and the first shell. If the displacements of each atom are independent of one another (an Einstein model), $\sigma_1^2 = 2\sigma_0^2$. If the motions are completely correlated, as would be the case for long wavelength vibrations, then $\sigma_1^2 = 0$. For Cu, $\sigma_0^2(300\,^\circ\mathrm{K}) - \sigma_0^2(77\,^\circ\mathrm{K}) = 0.00448$ from the measured Debye-Waller factor. This value is the same within experimental error as the EXAFS value and not a factor of 2 smaller, indicating that the vibration between nearest-neighbor atoms is partially correlated. Obviously for Cu, $N_2 = N_1$, so that the value of $N_2 = (1.05 \pm 0.03)N_1$ gives an estimate for the reliability of this method in determining coordination numbers. Alternately, the reason for the line in Fig. 7 not passing through the origin could be an error in estimating E_0, since a change in E_0 produces a horizontal shift in the line. Assuming all of the error in Fig. 7 is caused by E_0, we find a value of $E_0 = 10$ eV instead of the value -9.5 eV used in Table II.

We have also tried to perform this analysis on the second-shell data, but no reliable analysis could be performed because both the truncation errors and the noise are too large.

In Fig. 3(a), we see that the first three peaks of Cu are peaked negatively while the fourth peak is peaked positively.[16] The explanation of this feature has recently been suggested by Lee and Pendry[12] as due to multiple-scattering effects. They predict other multiple-scattering effects around the sixth shell. All of these multiple-scattering effects occur at distances greater than r_0 for Cu, as given in Table I.

Besides the first four shells, the most striking features in Figs. 3 and 4 occur between the origin and the first shell. The fact that these low-r features do not change amplitude with temperature, as do the various shells, indicates that they are not related to the positions of the atoms. The cause for these low-r features is presently unknown. Possibilities are contributions from the conduction electrons, contributions to EXAFS near the edge from effects which are not accounted for in Eq. (3) such as rapid variations of density of states, many-body effects, nonmonotonic variation of the atomic matrix element for x-ray absorption, or a systematic error in the measurements.

A similar analysis as led to Fig. 7 for the first shell of Cu can be done for the first shell of GeO_2. The result is shown in Fig. 8, giving a value of $\sigma^2 = (0.0000 \pm 0.0003)k^2 + 0 \pm 0.02$ due to disorder in the glassy state. This verifies quantitatively that the disorder of the tetrahedron of the oxygen first neighbors about the Ge atoms is quite small in the glassy state. As seen by the greatly decreased amplitude of the Ge peak in Fig. 5, appreciable disorder starts occurring only in the second shell. Also note that the fact that scattering from O has a more complicated phase shift variation than the linear one of Eq. (11) does not inhibit quantitative analysis.

At large r, the shells are close enough together so that the side lobes interfere with adjacent peaks, making peak indentification uncertain. The side lobes of the jth shell can be eliminated by deconvoluting the envelope due to scattering, disorder, and finite cutoff from the structural information. A successful deconvolution procedure has been developed recently for low-energy-electron-diffraction (LEED) data.[17] Such a technique may be helpful in separating the different shells at larger r, especially if σ_j is approximately independent of j for such r values.

C. Mean free path

The value of λ in Eq. (3) can be obtained from Eq. (12) by plotting the

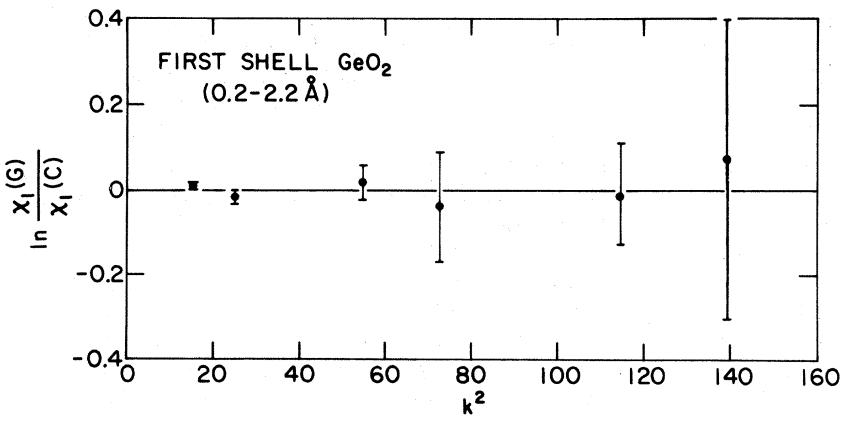

FIG. 8. Plot of $\ln|\chi_1^{(G)}/\chi_1^{(C)}|$ vs k^2. $\chi_1^{(G)}$ and $\chi_1^{(C)}$ are the inverse transforms of the first shells of oxygen surrounding the Ge atoms in glassy and crystalline GeO_2, respectively. Straight line satisfies the equation $k^2 = 0$.

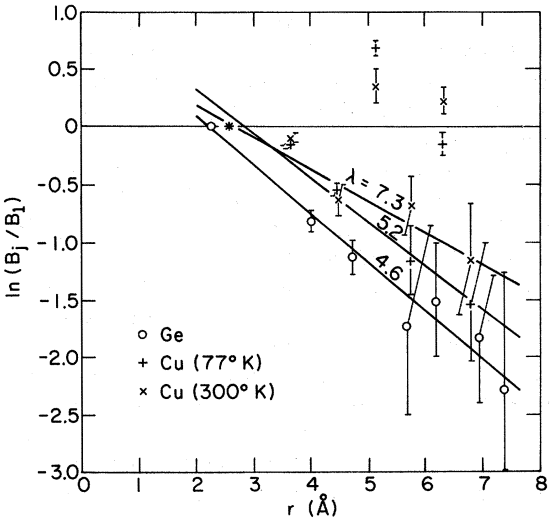

FIG. 9. $\ln(B_j/B_1)$ vs r (Å) for Ge and Cu at 77 and 300 °K, where $B_j = A_j R_j^2/N_j$. Data are tabulated in Table II. Slopes of the fitted lines give values of $\lambda = 4.6$, 5.2, and 7.3 Å for Ge, Cu (77 °K) and Cu (300 °K), respectively. Data points for the fourth and sixth shells in Cu deviate from a straight line because of multiple-scattering effects.

$$\ln\left(\frac{A_j R_j^2}{N_j} \Big/ \frac{A_1 R_1^2}{N_1}\right)$$

vs R_j, where A_j is the amplitude of the peak of the jth shell. If σ_j and t_j are independent of j, then such a plot should be a straight line whose slope is $-2/\lambda$. Such a plot is shown in Fig. 9 for Ge and Cu. The plot is approximately linear. Deviation from linearity and the different slopes at the two temperatures can be understood not only by the noise in the data but also by the fact that theoretically σ_j is expected to be different for various j, and this difference is a function of temperature. The effect of σ_j on the amplitude A_j would have to be eliminated to correctly determine λ. We have not done so. However, at liquid-nitrogen temperature, the effects of σ_j should be small enough so that the values of λ of 4.6 and 5.2 Å for Ge and Cu, respectively, are approximately correct. Note that for Cu, we did not use the points for the fourth and sixth coordination shells which are dominated by multiple-scattering effects.

Ashley and Doniach[18] have emphasized that λ is actually energy dependent increasing roughly as $(E)^{1/2}$ over the energy range of interest in EXAFS. If this is incorporated into Eq. (3), this would give an energy-dependent amplitude which would be different for each shell, so that, in principle, it would be possible to test this energy dependence by comparing the envelopes of various shells. Unfortunately, as described above, the data do not permit resolving the $t_j(2k)\, e^{-2\sigma_j^2 k^2}$ envelope beyond the first shell. Another way to determine the k dependence of λ is to vary the interval of k in the EXAFS data used to determine λ. For example, we analyzed the data over the interval from 2.74 to 10 Å^{-1}, and the value of λ so obtained is compared with the value obtained from the full interval of 2.74–15.8 Å^{-1}. The result is consistent with a $E^{1/2}$ dependence of λ, but the uncertainty is too great to distinguish from an energy-independent λ.

It is possible to compare the value of $\lambda = 5.2$ Å for Cu derived above with mean free paths derived from LEED data. Lee and Pendry[12] have used an imaginary part of the potential of 4 eV, which gives a range of $\lambda = 3.4$–12.7 Å over the energy range 50–700 eV. Our value should represent a weighted average of these values (8.9 Å) but is somewhat smaller. The values used by Lee and Pendry for the mean free path are in agreement with the average curve through a recent compilation of measurements on many different materials.[19] However, because of uncertainties in these measurements, our value of 5.2 Å for Cu is not inconsistent. While it is important to resolve the effects of the energy dependence of λ, in fact this dependence would mostly affect the determination of coordination numbers of faraway shells which cannot be accurately determined at this time in any case. The effect of λ can be minimized by comparing the EXAFS with standard compounds whose local environments are similar to the system being studied.

IV. SUMMARY AND DISCUSSION

In this paper, we have shown how a number of physical parameters may be derived from the Fourier transform of EXAFS data using the theoretical expression derived in I. It should be emphasized that this interpretation depends on the results of the single-scattering theory which was derived in a simple form by Sayers, Lytle, and Stern[20] and modified to a more general form by Stern.[1] The applicability of single-scattering theories and the assumptions used in their derivation have been analyzed recently by Lee and Pendry[12] and Ashley and Doniach.[18] Lee and Pendry have found that generally multiple-scattering effects are small. Exceptions occur when one shell of atoms is directly shadowed by an inner shell, in which case multiple-scattering effects will be large, because of forward scattering, and can even change the phase of the shell. This is seen in Cu for the fourth shell in Figs. 3 and 4 and in the deviation from the straight line of the fourth shell in Fig. 9. In the Fourier transform, multiple-scattering effects must always occur at distances greater than the first shell, so that the analysis used in this paper is always valid for the first shell. In prac-

tice, multiple-scattering effects are usually not important for the second and third shells, so that our analysis should usually apply to those shells also.

Interpretation of the data also depends on an understanding of the phase shifts. The assumption of a linear phase shift has been found to be valid for the heavier atoms in all of the covalent and metallically bonded systems studied. For the lighter atoms such as oxygen, the phase shift has a more complicated variation which reveals itself as an assymmetric function in r space in the Fourier transform of the EXAFS. A linear phase shift produces a transform which can be made symmetric or antisymmetric about a given shell. The location of the shell in the transform is shifted an amount α from the distance in real space because of the k dependence of the phase shift. All the evidence so far indicates that α is a characteristic of the excited atom that emits the photoelectron and the scattering atoms independent of their environment, for a given class of bonding. The class of bonding varies with the valence state and charge transferred to a given atom. If this result is verified by more exhaustive investigations, it would mean that α could be tabulated and used to determine the structure of unknown materials to an accuracy in the absolute location of atoms to 0.04 Å and in the relative position of atoms undergoing small displacements of 0.01 Å. Theoretical considerations are consonant with the constancy of α for a given atom in a given class of materials.

The usefulness of this important result still depends on the ability to determine into which class a given unknown material falls. Fortunately, the class of a material can be determined independently of EXAFS data. Both the energy shift of the absorption edge and the detailed structure of the absorption near the edge appear to be characteristic of the class of the material,[21] as one might expect theoretically. Thus the class of a given material can be determined by these means, and then the value of α can be unambiguously chosen from the tabulated values.

The inner potential E_0 introduces potentially the greatest uncertainty in the interpretation. By using as the transform ϕ_3 instead of ϕ_1, the effects of the uncertainty of E_0 are minimized. E_0 cannot be determined from the data in contrast to the phase shift. Fortunately, for expected uncertainties in E_0, the errors introduced in ϕ_3 in determining the location of atom and in the magnitude of the transforms are small. The quantity most sensitive to E_0 is β, the constant part of the phase shift, whose knowledge, fortunately, is not critical. In any case, standard compounds whose near-neighbor environment is similar to the system being studied can be used to determine the necessary parameters to obtain quantitative structural information, regardless of whether the phase shift is linear or not.

Of the parameters which can be determined from EXAFS, the distances from the absorbing atom to neighboring shells can be determined most accurately. We have also shown that relative measures of σ_j and N_j are possible in systems where there is additional structural or thermal disorder compared to a standard (e.g., amorphous versus crystalline GeO_2) for those shells which are isolated enough so that a large r-space interval may be retransformed into k space. This shell by shell retransforming also allows the envelope $t_j(2k) \times e^{-2\sigma_j^2 k^2}$ to be found. It should be possible to differentiate between different kinds of atoms because of differences in $t(2k)$, particularly in systems where the atoms are quite different (e.g., GeO_2).

Although there are still refinements in data acquisition and analysis which will allow a more complete and accurate determination of the physical parameters which affect EXAFS, this paper demonstrates that it is now possible to obtain useful and quantitative information in a wide variety of systems. The particular power of this technique is its capability of determining the environment about each atom separately. Its greatest usefulness should be in unraveling the characteristic of complicated structures with no long-range order such as in biological molecules[22] and commercially practical catalysts.[23]

---

*Research supported by the National Science Foundation.

[1]E. A. Stern, Phys. Rev. B 10, 3027 (1974).
[2]F. W. Lytle, D. E. Sayers, and E. A. Stern, preceding paper, Phys. Rev. B 11, 4825 (1975).
[3]D. E. Sayers, F. W. Lytle, E. A. Stern, Phys. Rev. Lett. 27, 204 (1971).
[4]E. A. Stern and D. E. Sayers, Phys. Rev. Lett. 30, 174 (1973).
[5]E. A. Stern, D. E. Sayers, F. W. Lytle, and P. A. Lee (unpublished).
[6]J. B. Pendry, J. Phys. C 2, 1215 (1969).
[7]D. W. Jepsen, P. M. Marcus, and F. Jona, Phys. Rev. B 5, 3933 (1972).
[8]E. A. Stern, Phys. Rev. B 7, 1303 (1973).
[9]M. Lax, Rev. Mod. Phys. 23, 287 (1951).
[10]J. B. Pendry, *Low Energy Electron Diffraction* (Academic, New York, 1974).
[11]G. Beni, P. Lee, and P. Platzmann (private communication.
[12]P. A. Lee and J. B. Pendry (unpublished).
[13]D. L. Mott, Ph.D. dissertation (University of New Mexico, 1963) (unpublished).
[14]P. A. Lee and D. E. Sayers (unpublished).
[15]J. Waser and V. Schomaker, Rev. Mod. Phys. 25, 671 (1953).
[16]The Cu transform shown in Ref. 4 contained a computational error which gave an incorrect r-dependent phase shift to the data.

[17]D. L. Adams and U. Landman, Phys. Rev. Lett. 33, 585 (1974).
[18]C. Ashley and S. Doniach (unpublished).
[19]C. J. Powell, Surf. Sci. 44, 29 (1974).
[20]D. E. Sayers, F. W. Lytle, and E. A. Stern, *Advances in X-ray Analysis* (Plenum, New York, 1970), Vol. 13, p. 248.
[21]F. W. Lytle, D. E. Sayers, and E. A. Stern (unpublished).
[22]D. E. Sayers, F. W. Lytle, M. Weissbluth, and P. Pianetta (unpublished).
[23]F. W. Lytle, D. E. Sayers, and E. B. Moore, Appl. Phys. Lett. 24, 45 (1974).